Supplementary Information

# Adaptive-to-Maladaptive Gradient of Emotion Regulation Tendencies are Embedded in the Functional-Structural Hybrid Connectome

Wonyoung Kim[1,2] & M. Justin Kim[2,3]

[1]Department of Psychology, Emory University, Atlanta, GA, USA
[2]Department of Psychology, Sungkyunkwan University, Seoul, South Korea
[3]Center for Neuroscience Imaging Research, Institute for Basic Science, Suwon, South Korea

**Supplementary Methods and Materials**

*Participants*

Data for this study was from the Max Planck Institute "Leipzig Study for Mind- Body-Emotion Interactions" (LEMON) dataset (Babayan et al., 2019). Recruited from September 2013 to September 2015, MRI data as well as data from behavioral tests, questionnaires, and interviews were collected from 227 eligible participants. Participants were excluded based on their current or history of cardiovascular (hypertension, heart attack, or congenital heart defect), psychiatric (with inpatient treatment for longer than 2 weeks, within the last 10 years, such as psychosis, attempted suicide, or post-traumatic stress disorder), neurological (multiple sclerosis, stroke, epilepsy, brain tumor, meningoencephalitis, or severe concussion), or malignant diseases, as well as medication or drug use (centrally active medication, beta- and alpha-blocker, cortisol, any chemotherapeutic or psychopharmacological medication, extensive alcohol, MDMA, amphetamines, cocaine, opiates, benzodiazepine, or cannabis) and standard MRI exclusion criteria. The dataset and its collection protocol are openly available to download at http://fcon_1000.projects.nitrc.org/indi/retro/MPI_LEMON.html. The LEMON dataset was collected adhering to the World Medical Association Declaration of Helsinki and was approved by the Ethics Committee of the University of Leipzig (reference number 154/13-ff).

Supplementary Information

The specific sample chosen for this study was young adults (20-30 years of age; n = 140). Among these young adults, participants were screened and excluded (n = 28) based on current or history of psychiatric diagnoses, assessed through Standardized Clinical Interview for DSM-IV or SCID-I (Saß, Wittchen, & Zaudig, 1996; Wittchen, Wunderlich, Gruschwitz, & Zaudig, 1997). Participants who had poor quality or missing data in structural, diffusion, or functional imaging data were also excluded (n = 6). Those with excessive head movement during resting state fMRI scans (mean framewise displacement, mean FD > 0.2 mm) were also screened (n = 4), as well as those who encountered errors during connectome construction (n = 3). The resulting sample comprised of 99 young German-speaking adults (n = 59 in age bracket 20-25, n = 40 in age bracket 25-30) among which 28 were female.

*Behavior Measures*

Data on emotion regulation tendency have been obtained from three different questionnaires (Emotion Regulation Questionnaire, ERQ; Cognitive Emotion Regulation Questionnaire, CERQ; Coping Orientations to Problems Experienced, COPE) to capture a broad range of individual difference in habitual emotion regulation. All questionnaires were German versions of the original scales. Of note, while some of the subscales from these questionnaires share the same name (e.g., "Acceptance" from CERQ and "Acceptance" from COPE), these were not considered redundant as the specific questionnaire items probed distinct aspects of habitual emotion regulation. As a result, the compiled emotion regulation tendency had 23 subscales that assessed emotion regulation tendencies in everyday life.

ERQ comprised of 10 items on a 7-point Likert scale ranging from 1 (strongly disagree) to 7 (strongly agree) (Abler & Kessler, 2009; Gross & John, 2003). Six items measured habitual

reappraisal, and four items gauged habitual expressive suppression. CERQ is a 5-point Likert scale questionnaire ranging from 0 (almost never) to 4 (almost always) with 27 items (Garnefski, Kraaij, & Spinhoven, 2001; Loch, Hiller, & Witthöft, 2011). The nine subscales of CERQ are acceptance, positive refocusing, refocusing on planning, positive reappraisal, putting into perspective, self-blame, rumination, catastrophizing, and blaming others. COPE (Brief COPE Inventory) was on a 4-point Likert scale ranging from 1 (not at all) to 4 (very much), and included subscales of self-distraction, use of emotional support, behavioral disengagement, positive reframing, humor, alcohol consumption, use of instrumental support, venting, planning, acceptance, self-blame, religion, denial, and active coping (Carver, 1997; Knoll, Rieckmann, & Schwarzer, 2005). Among the subscales of COPE, behavioral disengagement (Cronbach's alpha = 0.21) and planning (Cronbach's alpha = 0.44) were discarded due to poor reliability.

*Image Acquisition*

The following descriptions on image acquisition and preprocessing are further described in the original paper (Babayan et al., 2019). All MRI images were acquired from a 3-Tesla scanner (32-channel head coil, MAGNETOM Verio, Siemens Healthcare GmbH, Erlangen, Germany), and had a very large coverage using simultaneous multi-slice acquisition to include the brain and the cerebellum. Diffusion MRI data were collected parallel to the AC-PC line, with the volume at 149.6 mm height covering the entire brain including the cerebellum. Functional data were angulated by -15° backwards relative to the AC-PC line, in which the slice block at 147 mm height also covered the entire brain including the cerebellum.

T1-weighted images with 1mm isotropic voxel size were first collected through Magnetization-Prepared 2 Rapid Acquisition Gradient Echoes (MP2RAGE) sequence (Marques

et al., 2010).    A multiband accelerated sequence (Feinberg et al., 2010; Setsompop et al., 2012; Xu et al., 2013) combined with an in-plane GRAPPA (Griswold et al., 2002) (TR = 7,000 ms, TE = 80 ms, GRAPPA acceleration factor = 2, bandwidth = 1,502 Hz/Px, field of view = 220 × 220 mm$^2$, and voxel size = 1.7 × 1.7 × 1.7 mm$^3$) was used to attain 60 diffusion MRI images with seven b0 images (60 diffusion directions, b-value = 1000 s/mm$^2$).    Functional images were collected through a T2*-weighted gradient echo echo planar imaging (EPI) multiband BOLD resting state fMRI sequence (Feinberg et al., 2010; Xu et al., 2013; Moeller et al., 2010) (TR = 1400 ms, total number of volumes = 657, total acquisition time 15 min 30 s).    In the resting state sequence, the participants were instructed to remain awake and lie still with their eyes open while looking at a fixation cross.    One gradient echo fieldmap scan as well as two pairs of spin echo EPI images with reversed phase encoding direction were also acquired for correction for geometric distortions in EPI images.

*Image Preprocessing and Quality Check*

Preprocessed T1 MP2RAGE data were used as provided from the LEMON dataset.    In short, the background of the uniform T1-weighted image was removed using CBS Tools (Bazin et al., 2014).    Then, FreeSurfer's recon-all was used to reconstruct cortical surface from the masked image (Dale, Fischl, & Sereno, 1999; Fischl, Sereno, & Dale, 1999).    A brain mask was created based on the FreeSurfer segmentation results, and a spatial transformation between the individual's T1-weighted image and the Montreal Neurological Institute (MNI) 152 1mm standard space was computed via diffeomorphic nonlinear registration of the ANTs SyN algorithm (Avants et al., 2011).    A defacing mask was created using CBS Tools (Bazin et al., 2014) to be applied to all anatomical scans.

Supplementary Information

Diffusion-weighted images were preprocessed through FMRIB's Diffusion Toolbox (FDT) of FSL (FMRIB software library v6.0) in the following order (Jenkinson, Beckmann, Behrens, Woolrich, & Smith, 2012). First, using two volumes with reversed phase encoding, topup was carried out to correct for susceptibility-induced distortion (Andersson, Skare, & Ashburner, 2003). Second, brain was extracted using BET (Smith, 2002). Using *eddy* (–repol option), eddy current distortions as well as possible artifacts from head motion were identified and corrected (Andersson, Graham, Zsoldos, & Sotiropoulos, 2016; Andersson & Sotiropoulos, 2016).

QUAD and SQUAD, the automated quality control tool in FSL were used for quality checks on diffusion images (Bastiani et al., 2019). No participant was excluded based on the exclusion threshold of average volume-to-volume head motion of $< 3$ mm or $< 5\%$ of total outliers, adapted from previous literature (Zheng et al., 2021). The cleaned diffusion images were visually checked to confirm this result.

Functional images in the dataset were provided as preprocessed through a Nipype pipeline (Babayan et al., 2019; Mendes et al., 2019). In brief, the following steps were taken: discarding the first five EPI volumes, 3d motion correction (FSL MCFLIRT; Jenkinson, Bannister, Brady, & Smith, 2002), distortion correction (FSL FUGUE; Jenkinson, Beckmann, Behrens, Woolrich, & Smith, 2012), rigid-body coregistration of temporal mean image to anatomical image (FreeSurfer bbregister; Greve & Fischl, 2009), denoising (Nipype rapidart and aCompCor; Behzadi, Restom, Liau, & Liu, 2007), band-pass filtering between 0.01-0.1 Hz (FSL), mean-centering and variance normalization of the denoised time series (Nitime; Rokem, Trumpis, & Perez, 2009), and spatial normalization to MNI152 2-mm standard space (ANTs SyN; Avants et

al., 2011).    The preprocessing pipeline can be found at

https://github.com/NeuroanatomyAndConnectivity/pipelines/tree/master/src/lsd_lemon.

Quality assessment for functional images were performed through the *mriqc* package

(Esteban et al., 2017).    Apart from the eight participants that were excluded by the authors of

the original article before dataset distribution (ghosting artifact n = 2, incomplete scan n = 1,

anatomical preprocessing n = 4, functional preprocessing n = 1), four participants were further

excluded as noted above based on the conventional threshold for determining excessive head

movement (mean FD > 0.2 mm; 33).

*Building Connectomes*

The parcellation scheme used for both the functional and the structural connectomes was the

268-node Shen atlas (Shen, Tokoglu, Papademetris, & Constable, 2013), which is derived from

resting-state functional data of healthy adults.    The advantage of using this atlas is that it covers

the whole brain including the cortex, the subcortex, and the cerebellum, and also that it aids

translation of the results into the rich connectome-based predictive modelling literature that

utilize said atlas (Finn et al., 2015).    The Shen atlas was transformed into subject-specific

anatomical space using affine registration (FLIRT) and nonlinear registration (FNIRT) to be used

as masks for nodes (Jenkinson, Bannister, Brady, & Smith, 2002).

Structural connectomes were constructed with number of streamlines as the metric of

structural connectivity.    First, *bedpostx* and *probtrackx2* were performed on the cleaned

diffusion weighted images to draw white matter tracts connecting $268 \times 268$ pairs of regions in

subject-specific anatomical space (Behrens, Berg, Jbabdi, Rushworth, & Woolrich, 2007).    The

probabilistic tractography algorithm was set at 0.5-mm step length, 1,000 streamlines, and 2,000

steps across all computations.    Second, the raw number of streamlines were symmetrized and

log-transformed (Rosen & Halgren, 2021).   In detail, as white matter tracts were computed separately for both directions (e.g., region A to B, and region B to A), the arithmetic mean of these two values were used to symmetrize the structural connectome.   Lastly, log-transformation ($\log_{10}$) was carried out to account for the log-normally distributed probabilistic tractography results (Fornito, Zalesky, & Bullmore, 2016).

Functional connectomes were made using *3dNetCorr* in AFNI (Taylor & Saad, 2013). The algorithm first derives the mean timeseries of functional activations for each of the 268 regions, then calculates the correlation coefficients between the $268 \times 268$ pairs of regions for each subject.   These correlation coefficients, after Fisher z-transformation for normalization, are used as the metric of functional connectivity between pairs of regions.

Finally, functional-structural hybrid connectomes were created by combining the functional and the structural connectome following the procedures of previous literature (Amico & Goñi, 2018).   First, the Pearson correlation coefficient of the $i_{th}$ and $j_{th}$ row of the structural connectome are calculated, which effectively finds the "structural correlation."   Then, these structural correlation coefficients that imply the degree of similarity in structural connections with the rest of the brain constitute the new structural connectome.   Importantly, only connections that are unanimously connected across all participants are considered, which preserves the sparse matrix structure of the structural connectome.   This procedure ensures that the numeric distributions of the structural connectome are normalized to roughly match the functional connectome while also retaining the essential properties of the structural connectome (Amico & Goñi, 2018), much like the matching index (Rubinov & Sporns, 2010).

*Intersubject Representational Similarity Analysis*

Supplementary Information

To first confirm that the functional and structural connectome carry information relevant to emotion regulation tendencies, we conducted intersubject representational similarity analysis (IS-RSA) via Mantel tests (Finn et al., 2015; Mantel, 1967). IS-RSA examines the correlation between intersubject brain similarity (e.g., "do two subjects have similar connectomes?") and intersubject behavior similarity (e.g., "do two subjects have similar emotion regulation tendencies?"), which bypasses challenges that arise from directly comparing brain and behavior (e.g., "are $268 \times 268$ connectome values correlated to 23 emotion regulation strategy values?"). As such, the Spearman rank correlation between brain similarity matrix and behavior similarity matrix were tested in the IS-RSA framework. To elaborate, functional connectome similarity matrix was established by calculating the Euclidean distance between two vectors of functional connectome values for all pairs of individuals, resulting in a $99 \times 99$ matrix. Structural connectome similarity matrix and functional-structural hybrid connectome similarity matrix were constructed in identical manner. Statistical significance was investigated through the nonparametric procedure for Mantel tests, where the rows and columns of one of the similarity matrices are permuted 10,000 times to derive a null distribution of correlation values (Mantel, 1967). Data preprocessing, manipulation, and statistical analyses of IS-RSA were conducted through R 4.0.5 (R Core Team, 2021) and its package 'vegan' (Oksanen, 2010).

Through these analytical steps, we sought to examine whether the joint consideration of functional and structural connectomes, compared to either connectome separately, offered better explanatory power for individual differences in emotion regulation tendencies. We therefore tested three intersubject similarity correlation models: 1) interindividual similarity of functional connectome and interindividual similarity of emotion regulation tendencies, 2) interindividual similarity of structural connectome and interindividual similarity of emotion regulation

tendencies, and 3) interindividual similarity of functional-structural hybrid connectome and interindividual similarity of emotion regulation tendencies.

*Dimensionality Reduction*

Given that the functional-structural hybrid connectome showed stronger correlation with emotion regulation tendencies than either the functional or structural connectome by itself, the functional-structural hybrid connectome was further inspected to pinpoint the source of the correlation. Although canonical correlation analysis (CCA) is a powerful multivariate analytic tool for capturing covariance between two sets of variables with high dimensionality (i.e., $268 \times 268$ brain variables and 23 behavior variables) (McPherson, & Pestilli, 2021; Smith et al., 2015; Wang et al., 2020; Xia et al., 2018), concerns regarding its susceptibility to overfitting has been documented (Dinga et al., 2019; Mihalik et al., 2022). To circumvent this issue, we sought to reduce the dimensions of variables before they are entered into the CCA framework, which increases the stability and the reliability of CCA (Wang et al., 2020; Mihalik et al., 2022). Crucially, considering the number of subjects of our study (n = 99), the number of variables that would lead to reliable results is around 3 to 10 according to introductory texts (Tabachnick & Fidell, 2001; Pituch & Stevens, 2016) and less than 9 according to a recent methodological guide (Mihalik et al., 2022). Therefore, these standards were kept in mind when deciding the optimal number of dimensions in the following dimension reduction schemes.

Principal component analysis (PCA) was utilized to extract the principal components among the 23 dimensions of emotion regulation tendencies. In detail, principal axes that are orthogonal to each other were extracted in the order of amount of variance explained. It is worth noting that the 23 emotion regulation strategies were standardized because PCA is

sensitive to scaling differences that were present among the three distinct questionnaires. Maximizing consensus between multiple criteria on the number of components to retain (Lüdecke, Ben-Shachar, Patil, & Makowski, 2020), three principal components that accounted for the 38.4% of the variance among the 23 dimensions were derived (Supplementary Figure 1A). A seven-component solution also emerged as the second-best solution that explains 63.3% of the variance but was ultimately discarded due to risk of overfitting.

Independent component analysis (ICA) was chosen as the dimension reduction scheme for functional-structural hybrid connectomes. In practice, this would entail decomposing the variance of the functional-structural hybrid connectomes into a handful of components that each possess variance independent to each other. In other words, networks of functional and structural connections that covary would be clustered together to be separated from other networks. Adopting a previous approach (Amico & Goñi, 2018), the ICA procedure was carried out as follows. First, PCA was performed on the functional-structural hybrid connectomes to filter noise (Calhoun et al., 2006; Kessler, Angstadt, Welsh, & Sripada, 2014). This resulted in 42 components that explained 90% of variance in the data, which is comparable to the 40 components that explained 90% of variance in the original functional-structural hybrid connectome ICA study (Amico & Goñi, 2018). Then, the FastICA algorithm was run 1,000 times to extract the most robust components (Hyvärinen, 1999). The resultant components were only retained if they emerged more than 95% of the 1,000 runs with correlation higher than .95 across runs. It is worth noting that since it is challenging to anticipate the exact number of independent components that is adequate for the data at hand (Calhoun, Liu, & Adalı, 2009; Hyvärinen, & Oja, 2000), we chose to first run ICA under various settings. As the final number of independent components reached a plateau that indicate reliability at four and again at

sixteen across the manifold settings, a four-component solution was chosen to avoid overfitting (Supplementary Figure 1B).

*Control Analyses*

To account for possible alternate explanations for our results, we first carried out the CCA analysis with either the functional connectome or the structural connectome as sole source of information.  This entailed applying PCA and ICA to the functional connectome as well as applying PCA to the structural connectome to match the number of variables that would be entered into CCA.  Of note, because the structural connectome is relatively redundant between subjects (Amico & Goñi, 2018), PCA alone was enough to reduce the dimensionality down to 4 components, explaining 96% of variance.  This procedure was designed to check if significant canonical correlations could be derived from using only the functional or the structural connectome.

We additionally performed permutation tests where the entire ICA and CCA pipeline was repeated 1,000 times after permuting the combination of connectomes (Supplementary Figure 2). In detail, we reasoned that if the CCA result is solely dependent on 1) the functional connectome, 2) the structural connectome, or 3) the pure amount of data in the functional and structural connectome, it would not be robust to randomizing the functional-structural combinations across subjects.  We therefore mix-and-matched the functional and structural connectome pairs before entering them into the ICA and CCA pipeline 1,000 times to establish a null distribution of canonical correlation coefficients.  The number of independent components was set at 4 across all trials to keep the amount of variance consistent.

Supplementary Information

*HBN dataset connectome building*

The same 268-node Shen atlas parcellation scheme was used for both the functional and the structural connectomes for the HBN dataset as well (Shen, Tokoglu, Papademetris, & Constable, 2013). Following affine registration (FLIRT) and nonlinear registration (FNIRT), the Shen atlas was transformed into subject-specific anatomical space (Jenkinson, Bannister, Brady, & Smith, 2002).

Functional connectomes were built from resting state data. Collected from the Siemens 3T Prisma at Citigroup Biomedical Imaging Center (CBIC; n = 71) or from the Siemens 3T Tim Trio at Rutgers University Brain Imaging Center (RUBIC; n = 22), resting state scans ran for 5.1 minutes (TR = 800 ms; TE = 30 ms; FA = 31°; slice thickness = 2.4 mm; field of view (FOV) = 204 mm; multi-band acceleration factor = 6; voxel size = 2.4 mm isotropic). The fMRI data were preprocessed via fMRIPrep 21.0.2 (60), which includes BOLD signal reference image estimation, head-motion estimation, slice-time correction, co-registration, resampling onto standard space (MNI PediatricAsym:cohort-1) and confounds estimation. Smoothing was done as well with a 4 mm Full-Width at Half-Maximum Gaussian kernel using 3dmerge in AFNI (Cox, 1996; Cox & Hyde, 1997). After discarding the first four volumes, confound regression was also performed with 24 head motion parameters (three translational and three rotational deviations and their squares, six temporal derivatives and their squares) and three mean tissue signals (global, cerebrospinal fluid and white matter). Then, high-pass filtering and low-pass filtering were carried out with a 0.01 Hz cut-off and a 0.10 Hz cut-off. Finally, functional connectomes were constructed following the same steps as described above.

Structural connectomes for the HBN dataset were also made using number of streamlines as the metric of structural connectivity. Single-shell ($b$ = 1000 s/mm$^2$) dMRI scans

were acquired ($1.8 \times 1.8 \times 1.8$ mm$^3$; 72 slices; TE = 100.20 ms; TR = 3320 ms; flip angle = 90°; multiband acceleration factor 3; 64 diffusion directions). Further information on image acquisition can be found in the original paper for the dataset (Alexander et al., 2017). Four individuals from the dataset had missing diffusion imaging scans and were excluded from further analyses. Diffusion images were preprocessed using similar denoising and distortion correction methods as the young adult dataset (Andersson et al., 2003; Smith et al., 2004; Andersson & Sotiropoulos, 2016), but were processed through the MRtrix3 pipeline (Tournier et al., 2019). In detail, analyses were restricted to brain voxels (Tustison et al., 2010), and multi-tissue constrained spherical deconvolution was conducted to estimate multiple fiber orientations in each voxel (Jeurissen, Tournier, Dhollander, Connelly, & Sijbers, 2014), followed by calculation of fiber orientation density (Raffelt et al., 2017). Then, gray matter and white matter tissue boundaries were found on individual anatomical images and were coregistered with the diffusion images to anatomically constrain tractography (Smith, Tournier, Calamante, & Connelly, 2012). Finally, probabilistic tractography (iFOD2 algorithm; FOD cutoff 0.06, maximum tract length 250 mm, 10 million streamlines) was performed with the *tckgen* command (Tournier, Calamante, & Connelly, 2010). This resulted in structural connectomes with the $268 \times 268$ resolution, similar to the young adult dataset.

*Replication of the CCA results on HBN dataset*

Lastly, CCA was carried out using the functional and structural connectomes of the transdiagnostic adolescents following the same pipeline as described above. Adhering to the original parameters (i.e. retaining components appearing in more than 95% of the 1,000 runs with correlation higher than .95 across runs) yielded no stable independent components from the

functional-structural hybrid connectomes. Because more lenient thresholds of 50% appearance and .50 correlation across runs was found to be sufficient in finding robust components (Amico & Goñi, 2018), we then lowered both thresholds to 85% appearance and .85 correlation to explore the possibility that connectomes of individuals with diverse clinical symptoms are more variable and require more flexibility. This resulted in four independent components of functional-structural connectomes following the same decision heuristic. The first three principal components (explaining 63.9% of variance; Supplementary Table 2) of coping strategies were used as input data for the CCA analysis (Supplementary Figure 4). This decision was based on an observation that despite the high percentage of variance explained by the first principal component of the CCSC scale, it may be insufficient in considering the variable nature of coping strategies, as the low loadings across strategies imply (Table 2). The covariate matrix comprised of gender, age, data acquisition site, resting-state EPI movement (mean FD values), and diagnoses categories were regressed out from both the ICA components and the PCA components. The permutation and significance testing procedure followed the same pipeline, which yielded a canonical correlation between the functional-structural hybrid connectomes and coping strategies after correcting for multiple tests.

**Supplementary Results**

*Intersubject Representational Analysis*

Mantel tests with 10,000 permutations revealed that interindividual similarity of the functional-structural hybrid connectome was significantly correlated with interindividual similarity of

emotion regulation tendency ($P = 0.002$).   The structural connectome similarity matrix was not significantly correlated with emotion regulation tendency similarity matrix ($P = 0.116$).   The functional connectome similarity matrix was significantly correlated with emotion regulation tendency similarity matrix ($P = 0.029$).   When comparing the mantel correlation coefficient, functional-structural hybrid connectome similarity was highest (*Mantel's r* $= 0.141$) compared to functional connectome similarity (*Mantel's r* $= 0.092$) and structural connectome similarity (*Mantel's r* $= 0.067$).   Furthermore, functional-structural hybrid connectome similarity was still significantly correlated with emotion regulation tendency similarity even after controlling for either the functional connectome similarity ($P = 0.025$) or the structural connectome similarity ($P = 0.009$).

*Dimensionality Reduction*

Performing PCA on the 23 emotion regulation strategies led to three principal components that explained 38.4% of variance.   To elaborate, the first component loaded most positively on positive reappraisal, use of instrumental support, and refocus on planning, and loaded most negatively on suppression, substance use, and catastrophizing (15.1% variance explained).   The second component had heavy positive loadings on catastrophizing, denial, and rumination, when loading negatively on positive reframing, reappraisal, and positive reappraisal (13.6% variance explained).   The last component loaded positively on suppression, acceptance (both CERQ and COPE), and self-blame (both CERQ and COPE), and loaded negatively on venting, use of emotional support, and use of instrumental support (9.8% variance explained).   Consequently, the three principal components of emotion regulation tendencies were each deemed to carry unique aspects (Supplementary Table 1).

Supplementary Information

ICA on the 99 pairs of functional-structural hybrid connectomes resulted in four

independent components that convey network covariance properties across the functional and

structural connectome (Supplementary Figure 3).   The first independent component consisted of

functional connections involving the default mode network and the medial frontal network as

well as structural connections mainly concerning the motor network and the visual network.

The second independent component had functional connections focused within the medial frontal

network, frontoparietal network, and the default mode network and structural connections

heavily involving subcortical and cerebellar regions.   The functional component of the third

independent component heavily engaged the visual networks and the motor network, whereas the

structural component was concentrated on the subcortical-cerebellum network and the visual

networks.   The fourth independent component had pronounced functional connections

involving the medial frontal network, frontoparietal network, the default mode network, and the

visual networks as well as structural connections associated with the subcortical-cerebellum

network, the motor network, and the visual networks.


*Control Analysis*

First, we tested if either the functional connectome or the structural connectome was sufficient to

extract a significant correlation between brain variables and emotion regulation tendency

variables.   CCA analyses showed no significant mode of correlation between brain components

and emotion regulation tendency components when using either the functional connectome ($P =$

0.340) or the structural connectome ($P = 0.229$) alone.

Among the 1,000 trials of permutations, the canonical correlation coefficient of the true

CCA result was at the top 44, indicating that the true combination of the functional and structural

connectomes significantly contributed to the CCA result ($P = 0.044$).   In other words, the result

was not driven solely by the functional connectome, the structural connectome, or the pure

amount of data in the functional and structural connectome.

*Replication of the CCA results on HBN dataset*

CCA results indicated a significant canonical correlation based on 10,000 permutations ($r =$

0.331, $P = 0.042$ after correcting for multiple tests; Supplementary Figure 4).   When combined

across the independent components of the functional-structural hybrid connectomes using the

resultant CCA weights, the composite mode mainly involved functional connections between the

medial frontal network and other networks as well as connections within the visual network

(Supplementary Figure 5).   Critical structural connections from the composite mode were

aggregated in the subcortical-cerebellum network and between the visual networks and other

networks.   The composite coping tendency followed a similar adaptive-to-maladaptive

spectrum (Supplementary Table 2).

Notably, the composite coping tendency score comprised of the first three first principal

components had a stronger correlation with the network score derived from the young adult

sample ($r = 0.291$, $P = 0.006$).   The difference in model fit showed that the composite coping

tendency score better explained the network score ($\Delta AIC = 2.53$; Burnham & Anderson, 2004).

This indicates that including a wider range in the adaptive-to-maladaptive spectrum of coping

strategies leads to stronger alignment with the originally derived network, which bolsters the

rationale for utilizing the first three principal components for the CCA analysis.
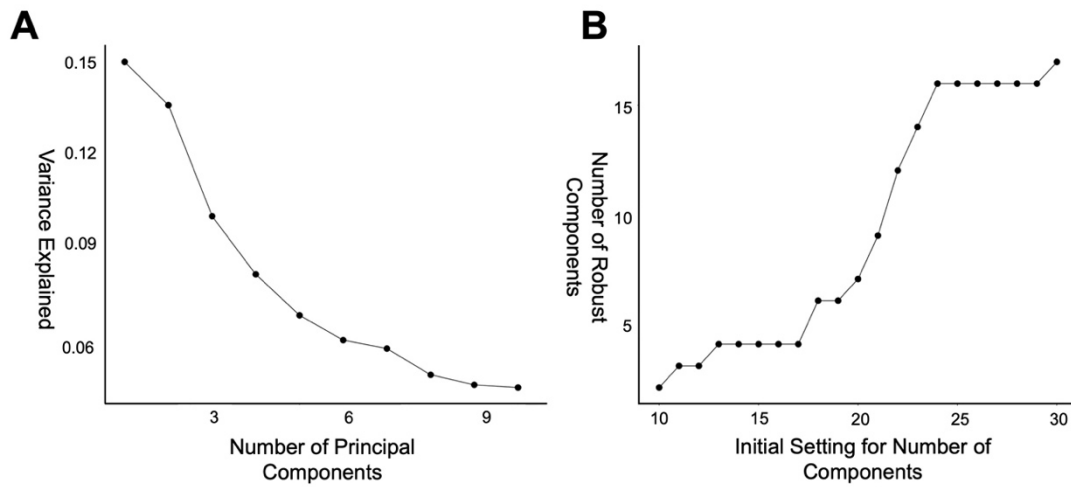
**Supplementary Figure 1**. Finding the optimal number of components in the dimensionality reduction process.    **A** In the PCA procedure for 23 emotion regulation strategies, a 3-component solution emerged as a solution that maximizes consensus among various criteria, followed by a 7-component solution, both of which can be confirmed by the "elbow" points in the scree plot. **B** In the ICA procedure for functional-structural hybrid connectomes, highest reliability was shown by the 4-robust-component solution and the 16-robust-component solution.    The x-axis specifies the initial setting for number of components, which is used to extract a specific number of independent components before finding the most robust components among them.
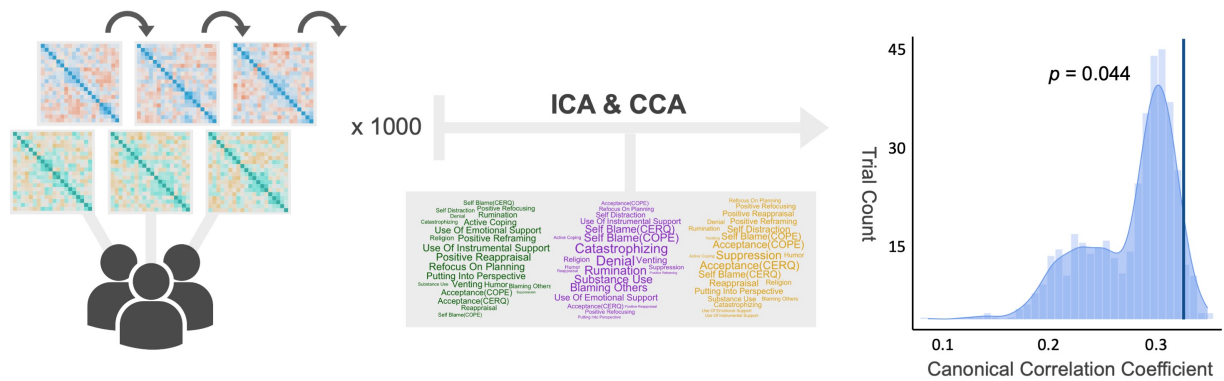
**Supplementary Figure 2**. Permutation test. Functional-structural pairings were mix-and-matched through permutation and were subjected to the ICA and CCA pipeline to create a null distribution of CCA results.    The true CCA result was statistically significant ($P = 0.044$), indicating that the result was not solely driven by 1) the functional connectome, 2) the structural connectome, or 3) the amount of data in the functional-structural hybrid connectome.
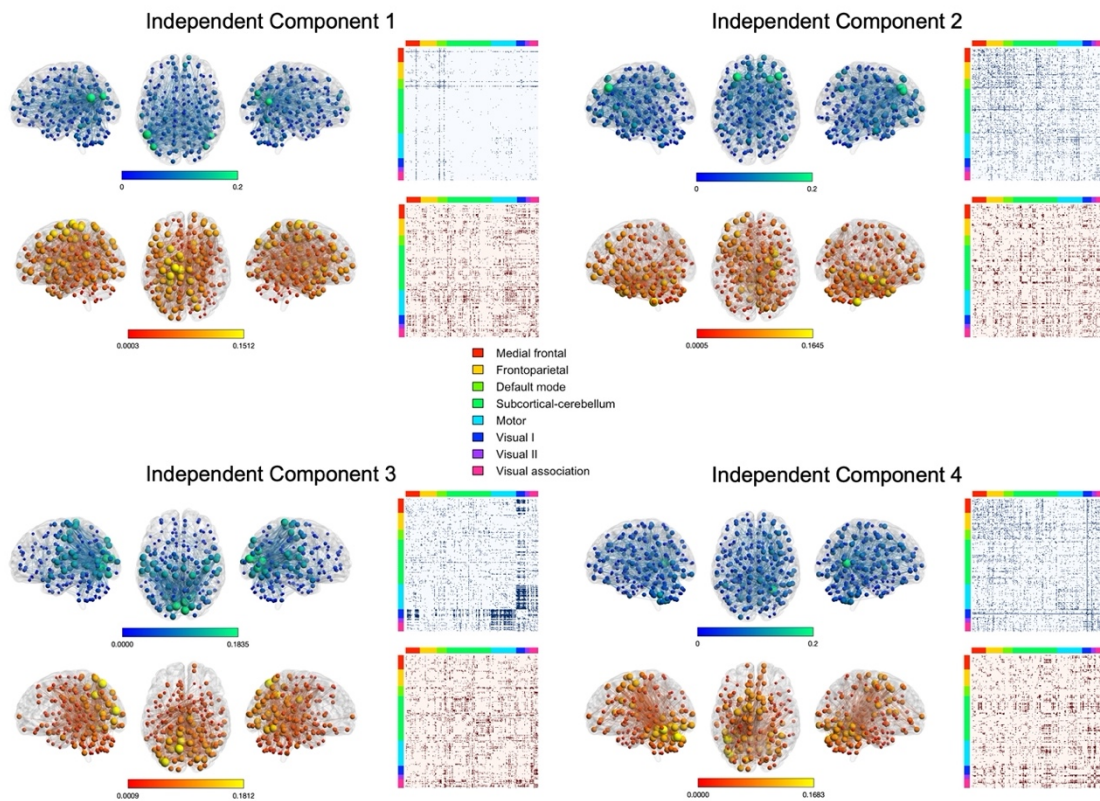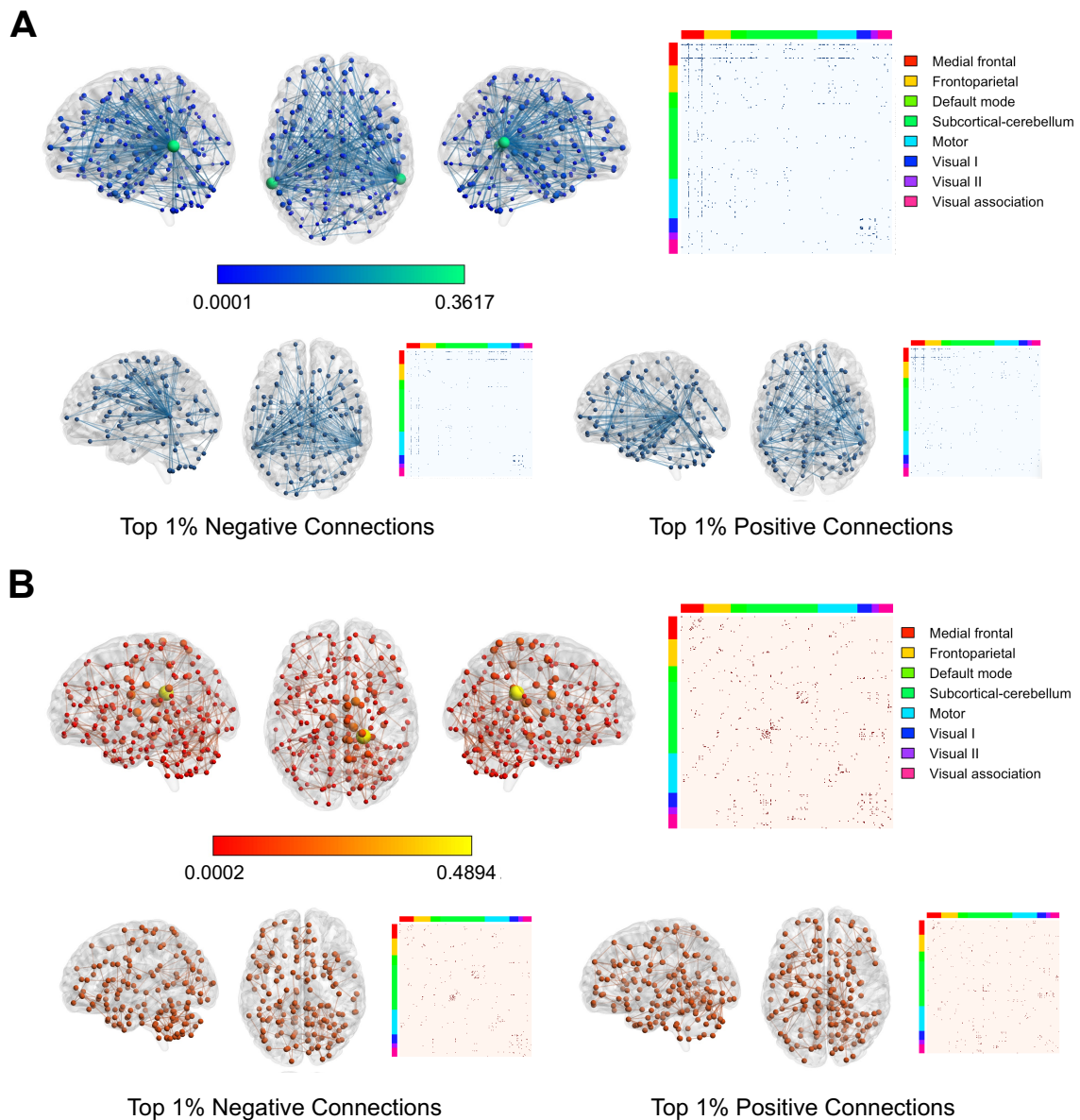
**Supplementary Figure 3**. Four independent components of the functional-structural hybrid connectome. Sizes and colors of the nodes are scaled by their eigenvector centrality (Rubinov & Sporns, 2010). To allow comparison between components, the maximum eigenvector centrality value for color scaling was set at 0.2 for the functional portions of independent component 1, 2, and 4. Connections with top 1% weight in either the positive or the negative direction are illustrated in the brain figures and the matrices.
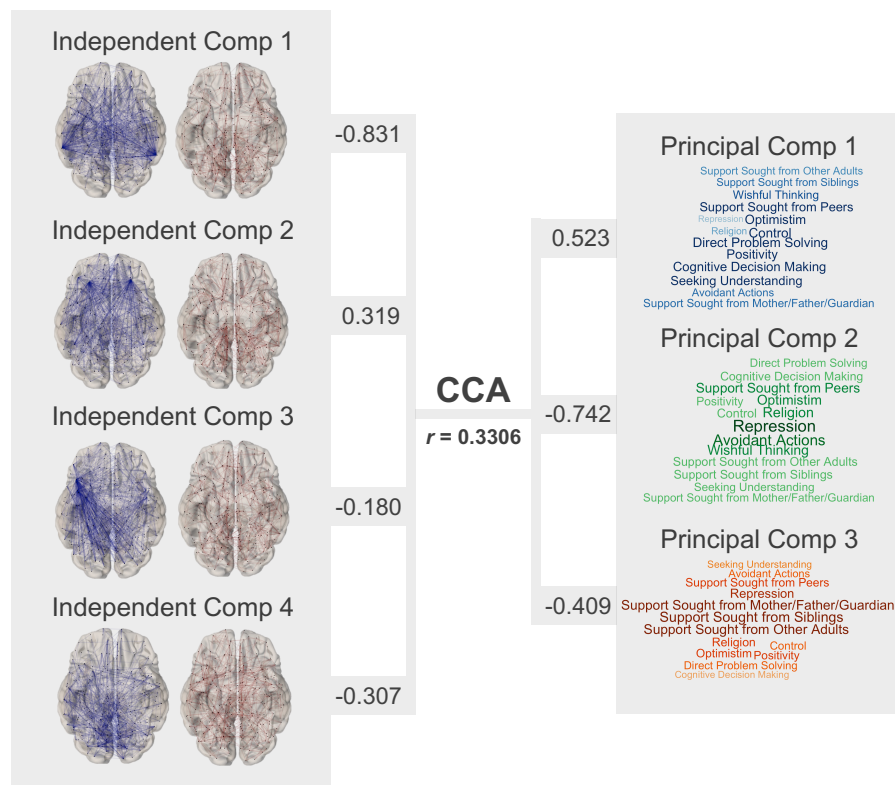
**Supplementary Figure 4**. Replication of the CCA framework in the HBN dataset. After correcting for multiple tests, one significant mode of correlation was found between the functional-structural hybrid connectomes and the coping strategies of the adolescents.

**A**



0.0001          0.3617

Medial frontal
Frontoparietal
Default mode
Subcortical-cerebellum
Motor
Visual I
Visual II
Visual association

Top 1% Negative Connections          Top 1% Positive Connections

**B**



0.0002          0.4894

Medial frontal
Frontoparietal
Default mode
Subcortical-cerebellum
Motor
Visual I
Visual II
Visual association

Top 1% Negative Connections          Top 1% Positive Connections

**Supplementary Figure 5.** Composite functional and structural network properties from the significant mode of canonical correlation in the HBN dataset. **A** Important functional connections were located between the medial frontal network and other networks as well as within the visual network. **B** Important structural connections involved the subcortical-cerebellum network and the visual networks.

Supplementary Information

**Supplementary Table 1**. Three principal components of 23 emotion regulation strategies. Weights show the degree to which each emotion regulation tendency is involved in the principal components.

| Emotion Regulation Strategies | PC1 | PC2 | PC3 |
|---|---|---|---|
| Reappraisal | 0.125 | -0.167 | 0.239 |
| Suppression | -0.193 | 0.028 | 0.388 |
| Self Blame(CERQ) | 0.073 | 0.261 | 0.273 |
| Acceptance(CERQ) | 0.215 | 0.032 | 0.362 |
| Rumination | 0.195 | 0.333 | 0.007 |
| Positive Refocusing | 0.115 | -0.017 | 0.060 |
| Refocus On Planning | 0.334 | -0.006 | -0.064 |
| Positive Reappraisal | 0.349 | -0.211 | 0.141 |
| Putting Into Perspective | 0.292 | -0.149 | 0.181 |
| Catastrophizing | 0.012 | 0.375 | 0.070 |
| Blaming Others | 0.086 | 0.285 | -0.091 |
| Self Distraction | 0.052 | 0.094 | 0.248 |
| Use Of Emotional Support | 0.280 | 0.175 | -0.226 |
| Positive Reframing | 0.288 | -0.239 | 0.151 |
| Humor | 0.205 | -0.064 | 0.045 |
| Substance Use | -0.065 | 0.301 | 0.090 |
| Use Of Instrumental Support | 0.327 | 0.124 | -0.242 |
| Venting | 0.269 | 0.187 | -0.258 |
| Acceptance(COPE) | 0.219 | -0.034 | 0.312 |
| Self Blame(COPE) | 0.007 | 0.291 | 0.257 |
| Religion | 0.122 | 0.086 | 0.086 |
| Denial | 0.017 | 0.389 | 0.014 |
| Active Coping | 0.246 | -0.113 | -0.260 |

**Supplementary Table 2.** Three principal components of 14 coping strategies and the composite coping tendency derived from the results of the CCA analysis on the transdiagnostic adolescent dataset. The 14 coping strategies are shown ordered by their canonical correlation weight.

| Coping Strategies | Weight | PC1 | PC2 | PC3 |
|---|---|---|---|---|
| Seeking Understanding | 0.445 | 0.298 | -0.229 | -0.291 |
| Cognitive Decision Making | 0.405 | 0.312 | -0.129 | -0.358 |
| Direct Problem Solving | 0.375 | 0.326 | -0.233 | -0.076 |
| Positivity | 0.274 | 0.314 | -0.156 | 0.013 |
| Control | 0.241 | 0.325 | -0.080 | -0.029 |
| Wishful Thinking | 0.162 | 0.256 | 0.190 | -0.416 |
| Support Sought from Mother/Father/Guardian | 0.159 | 0.243 | -0.250 | 0.375 |
| Support Sought from Peers | 0.034 | 0.298 | 0.133 | 0.562 |
| Support Sought from Other Adults | 0.030 | 0.214 | -0.104 | 0.390 |
| Optimism | 0.016 | 0.310 | 0.170 | 0.049 |
| Support Sought from Siblings | -0.002 | 0.221 | -0.110 | 0.486 |
| Religion | -0.130 | 0.176 | 0.241 | 0.107 |
| Avoidant Actions | -0.145 | 0.225 | 0.421 | -0.120 |
| Repression | -0.513 | 0.133 | 0.666 | 0.217 |

## References

Abler, B., & Kessler, H. (2009). Emotion regulation questionnaire–Eine deutschsprachige Fassung des ERQ von Gross und John. *Diagnostica*, *55*(3), 144-152. doi: https://doi.org/10.1026/0012-1924.55.3.144

Alexander, L. M., Escalera, J., Ai, L., Andreotti, C., Febre, K., Mangone, A., ... & Milham, M. P. (2017). An open resource for transdiagnostic research in pediatric mental health and learning disorders. *Scientific data*, *4*(1), 1-26. doi: https://doi.org/10.1038/sdata.2017.181

Amico, E., & Goñi, J. (2018). Mapping hybrid functional-structural connectivity traits in the human connectome. *Network Neuroscience*, *2*(3), 306-322. doi: https://doi.org/10.1162/netn_a_00049

Andersson, J. L., & Sotiropoulos, S. N. (2016). An integrated approach to correction for off-resonance effects and subject movement in diffusion MR imaging. *Neuroimage*, *125*, 1063-1078. doi: https://doi.org/10.1016/j.neuroimage.2015.10.019

Andersson, J. L., Graham, M. S., Zsoldos, E., & Sotiropoulos, S. N. (2016). Incorporating outlier detection and replacement into a non-parametric framework for movement and distortion correction of diffusion MR images. *Neuroimage*, *141*, 556-572. doi: https://doi.org/10.1016/j.neuroimage.2016.06.058

Andersson, J. L., Skare, S., & Ashburner, J. (2003). How to correct susceptibility distortions in spin-echo echo-planar images: application to diffusion tensor imaging. *Neuroimage*, *20*(2), 870-888. doi: https://doi.org/10.1016/S1053-8119(03)00336-7

Avants, B. B., Tustison, N. J., Song, G., Cook, P. A., Klein, A., & Gee, J. C. (2011). A reproducible evaluation of ANTs similarity metric performance in brain image registration. *Neuroimage*, *54*(3), 2033-2044. doi: https://doi.org/10.1016/j.neuroimage.2010.09.025

Babayan, A., Erbey, M., Kumral, D., Reinelt, J. D., Reiter, A. M., Röbbig, J., ... & Villringer, A. (2019). A mind-brain-body dataset of MRI, EEG, cognition, emotion, and peripheral physiology in young and old adults. *Scientific data*, *6*(1), 1-21. doi: https://doi.org/10.1038/sdata.2018.308

Supplementary Information

Bastiani, M., Cottaar, M., Fitzgibbon, S. P., Suri, S., Alfaro-Almagro, F., Sotiropoulos, S. N., ... & Andersson, J. L. (2019). Automated quality control for within and between studies diffusion MRI data using a non-parametric framework for movement and distortion correction. *Neuroimage*, *184*, 801-812. doi: https://doi.org/10.1016/j.neuroimage.2018.09.073

Bazin, P. L., Weiss, M., Dinse, J., Schäfer, A., Trampel, R., & Turner, R. (2014). A computational framework for ultra-high resolution cortical segmentation at 7 Tesla. *NeuroImage*, *93*, 201-209. doi: https://doi.org/10.1016/j.neuroimage.2013.03.077

Behrens, T. E., Berg, H. J., Jbabdi, S., Rushworth, M. F., & Woolrich, M. W. (2007). Probabilistic diffusion tractography with multiple fibre orientations: What can we gain?. *neuroimage*, *34*(1), 144-155. doi: https://doi.org/10.1016/j.neuroimage.2006.09.018

Behzadi, Y., Restom, K., Liau, J., & Liu, T. T. (2007). A component based noise correction method (CompCor) for BOLD and perfusion based fMRI. *Neuroimage*, *37*(1), 90-101. doi: https://doi.org/10.1016/j.neuroimage.2007.04.042

Burnham, K. P., & Anderson, D. R. (2004). Multimodel inference: understanding AIC and BIC in model selection. *Sociological methods & research*, *33*(2), 261-304. doi: https://doi.org/10.1177/0049124104268644

Calhoun, V. D., Adali, T., Giuliani, N. R., Pekar, J. J., Kiehl, K. A., & Pearlson, G. D. (2006). Method for multimodal analysis of independent source differences in schizophrenia: combining gray matter structural and auditory oddball functional data. *Human brain mapping*, *27*(1), 47-62. doi: https://doi.org/10.1002/hbm.20166

Calhoun, V. D., Liu, J., & Adalı, T. (2009). A review of group ICA for fMRI data and ICA for joint inference of imaging, genetic, and ERP data. *Neuroimage*, *45*(1), S163-S172.

Carver, C. S. (1997). You want to measure coping but your protocol's too long: Consider the brief cope. *International journal of behavioral medicine*, *4*(1), 92-100. doi: https://doi.org/10.1016/j.neuroimage.2008.10.057

Cox, R. W. (1996). AFNI: software for analysis and visualization of functional magnetic resonance neuroimages. *Computers and Biomedical Research*, 29(3), 162-173. doi: https://doi.org/10.1006/cbmr.1996.0014

Supplementary Information

Cox, R. W., & Hyde, J. S. (1997). Software tools for analysis and visualization of fMRI
data. *NMR in Biomedicine: An International Journal Devoted to the Development and
Application of Magnetic Resonance In Vivo*, *10*(4-5), 171-178. doi: 10.1002/(sici)1099-
1492(199706/08)10:4/5<171::aid-nbm453>3.0.co;2-l

Dale, A. M., Fischl, B., & Sereno, M. I. (1999). Cortical surface-based analysis: I. Segmentation
and surface reconstruction. *Neuroimage*, *9*(2), 179-194. doi:
https://doi.org/10.1006/nimg.1998.0395

Dinga, R., Schmaal, L., Penninx, B. W., van Tol, M. J., Veltman, D. J., van Velzen, L., ... &
Marquand, A. F. (2019). Evaluating the evidence for biotypes of depression:
Methodological replication and extension of. *NeuroImage: Clinical*, *22*, 101796. doi:
https://doi.org/10.1016/j.nicl.2019.101796

Esteban, O., Birman, D., Schaer, M., Koyejo, O. O., Poldrack, R. A., & Gorgolewski, K. J.
(2017). MRIQC: Advancing the automatic prediction of image quality in MRI from
unseen sites. *PloS one*, *12*(9), e0184661. doi:
https://doi.org/10.1371/journal.pone.0184661

Esteban, O., Markiewicz, C. J., Blair, R. W., Moodie, C. A., Isik, A. I., Erramuzpe, A., ... &
Gorgolewski, K. J. (2019). fMRIPrep: a robust preprocessing pipeline for functional
MRI. *Nature methods*, *16*(1), 111-116. doi: https://doi.org/10.1038/s41592-018-0235-4

Feinberg, D. A., Moeller, S., Smith, S. M., Auerbach, E., Ramanna, S., Glasser, M. F., ... &
Yacoub, E. (2010). Multiplexed echo planar imaging for sub-second whole brain FMRI
and fast diffusion imaging. *PloS one*, *5*(12), e15710. doi:
https://doi.org/10.1371/journal.pone.0015710

Finn, E. S., Glerean, E., Khojandi, A. Y., Nielson, D., Molfese, P. J., Handwerker, D. A., &
Bandettini, P. A. (2020). Idiosynchrony: From shared responses to individual
differences during naturalistic neuroimaging. *NeuroImage*, *215*, 116828. doi:
https://doi.org/10.1016/j.neuroimage.2020.116828

Finn, E. S., Shen, X., Scheinost, D., Rosenberg, M. D., Huang, J., Chun, M. M., ... & Constable,
R. T. (2015). Functional connectome fingerprinting: identifying individuals using
patterns of brain connectivity. *Nature neuroscience*, *18*(11), 1664-1671. doi:
https://doi.org/10.1038/nn.4135

Supplementary Information

Fischl, B., Sereno, M. I., & Dale, A. M. (1999). Cortical surface-based analysis: II: inflation, flattening, and a surface-based coordinate system. *Neuroimage*, *9*(2), 195-207. doi: https://doi.org/10.1006/nimg.1998.0396

Fornito, A., Zalesky, A., & Bullmore, E. (2016). *Fundamentals of brain network analysis*. Academic press.

Garnefski, N., Kraaij, V., & Spinhoven, P. (2001). Negative life events, cognitive emotion regulation and emotional problems. *Personality and Individual differences*, *30*(8), 1311-1327. doi: https://doi.org/10.1016/S0191-8869(00)00113-6

Greve, D. N., & Fischl, B. (2009). Accurate and robust brain image alignment using boundary-based registration. *Neuroimage*, *48*(1), 63-72. doi: https://doi.org/10.1016/j.neuroimage.2009.06.060

Griswold, M. A., Jakob, P. M., Heidemann, R. M., Nittka, M., Jellus, V., Wang, J., ... & Haase, A. (2002). Generalized autocalibrating partially parallel acquisitions (GRAPPA). *Magnetic Resonance in Medicine: An Official Journal of the International Society for Magnetic Resonance in Medicine*, *47*(6), 1202-1210. doi: https://doi.org/10.1002/mrm.10171

Gross, J. J., & John, O. P. (2003). Individual differences in two emotion regulation processes: implications for affect, relationships, and well-being. *Journal of personality and social psychology*, *85*(2), 348. doi: https://psycnet.apa.org/doi/10.1037/0022-3514.85.2.348

Hyvärinen, A. (1999). Fast ICA for noisy data using Gaussian moments. In *1999 IEEE international symposium on circuits and systems (ISCAS)* (Vol. 5, pp. 57-61). IEEE. doi: 10.1109/ISCAS.1999.777510.

Hyvärinen, A., & Oja, E. (2000). Independent component analysis: algorithms and applications. *Neural networks*, *13*(4-5), 411-430. doi: https://doi.org/10.1016/S0893-6080(00)00026-5

Jenkinson, M., Bannister, P., Brady, M., & Smith, S. (2002). Improved optimization for the robust and accurate linear registration and motion correction of brain images. *Neuroimage*, *17*(2), 825-841. doi: https://doi.org/10.1006/nimg.2002.1132

Jenkinson, M., Beckmann, C. F., Behrens, T. E., Woolrich, M. W., & Smith, S. M. (2012). Fsl. *Neuroimage*, *62*(2), 782-790. doi: https://doi.org/10.1016/j.neuroimage.2011.09.015

Supplementary Information

Jeurissen, B., Tournier, J. D., Dhollander, T., Connelly, A., & Sijbers, J. (2014). Multi-tissue constrained spherical deconvolution for improved analysis of multi-shell diffusion MRI data. NeuroImage, 103, 411-426. doi: https://doi.org/10.1016/j.neuroimage.2014.07.061

Kessler, D., Angstadt, M., Welsh, R. C., & Sripada, C. (2014). Modality-spanning deficits in attention-deficit/hyperactivity disorder in functional networks, gray matter, and white matter. *Journal of Neuroscience*, *34*(50), 16555-16566. doi: https://doi.org/10.1523/JNEUROSCI.3156-14.2014

Knoll, N., Rieckmann, N., & Schwarzer, R. (2005). Coping as a mediator between personality and stress outcomes: a longitudinal study with cataract surgery patients. *European Journal of Personality*, *19*(3), 229-247. doi: https://doi.org/10.1002/per.546

Loch, N., Hiller, W., & Witthöft, M. (2011). Der cognitive emotion regulation questionnaire (CERQ). *Zeitschrift für Klinische Psychologie und Psychotherapie*. doi: https://doi.org/10.1026/1616-3443/a000079

Lüdecke, D., Ben-Shachar, M. S., Patil, I., & Makowski, D. (2020). Extracting, computing and exploring the parameters of statistical models using R. *Journal of Open Source Software*, *5*(53), 2445. doi: https://doi.org/10.21105/joss.02445

Mantel, N. (1967). The detection of disease clustering and a generalized regression approach. *Cancer research*, *27*(2_Part_1), 209-220.

Marques, J. P., Kober, T., Krueger, G., van der Zwaag, W., Van de Moortele, P. F., & Gruetter, R. (2010). MP2RAGE, a self bias-field corrected sequence for improved segmentation and T1-mapping at high field. *Neuroimage*, *49*(2), 1271-1281. doi: https://doi.org/10.1016/j.neuroimage.2009.10.002

McPherson, B. C., & Pestilli, F. (2021). A single mode of population covariation associates brain networks structure and behavior and predicts individual subjects' age. *Communications Biology*, *4*(1), 943. doi: https://doi.org/10.1038/s42003-021-02451-0

Mendes, N., Oligschläger, S., Lauckner, M. E., Golchert, J., Huntenburg, J. M., Falkiewicz, M., ... & Margulies, D. S. (2019). A functional connectome phenotyping dataset including cognitive state and personality measures. *Scientific data*, *6*(1), 1-19. doi: https://doi.org/10.1038/sdata.2018.307

Mihalik, A., Chapman, J., Adams, R. A., Winter, N. R., Ferreira, F. S., Shawe-Taylor, J., ... & Alzheimer's Disease Neuroimaging Initiative. (2022). Canonical correlation analysis

and partial least squares for identifying brain-behaviour associations: a tutorial and a comparative study. *Biological Psychiatry: Cognitive Neuroscience and Neuroimaging*. doi: https://doi.org/10.1016/j.bpsc.2022.07.012

Moeller, S., Yacoub, E., Olman, C. A., Auerbach, E., Strupp, J., Harel, N., & Uğurbil, K. (2010). Multiband multislice GE-EPI at 7 tesla, with 16-fold acceleration using partial parallel imaging with application to high spatial and temporal whole-brain fMRI. *Magnetic resonance in medicine*, *63*(5), 1144-1153. doi: https://doi.org/10.1002/mrm.22361

Oksanen, J. (2010). Vegan: community ecology package. *http://CRAN. R-project. org/package= vegan*. Accessed 22 October 2021.

Pituch, K. A., & Stevens, J. P. (2016). *Applied multivariate statistics for the social sciences: Analyses with SAS and IBM's SPSS*. Routledge.

Power, J. D., Mitra, A., Laumann, T. O., Snyder, A. Z., Schlaggar, B. L., & Petersen, S. E. (2014). Methods to detect, characterize, and remove motion artifact in resting state fMRI. *Neuroimage*, *84*, 320-341. doi: https://doi.org/10.1016/j.neuroimage.2013.08.048

R Core Team (2021) R: A language and environment for statistical computing. (R Foundation for Statistical Computing, Vienna, Austria, 2021). https://www.R-project.org/. Accessed 10 September 2021.

Raffelt, D. A., Tournier, J. D., Smith, R. E., Vaughan, D. N., Jackson, G., Ridgway, G. R., & Connelly, A. (2017). Investigating white matter fibre density and morphology using fixel-based analysis. *Neuroimage*, *144*, 58-73. doi: https://doi.org/10.1016/j.neuroimage.2016.09.029

Rokem, A., Trumpis, M., & Perez, F. (2009). Nitime: time-series analysis for neuroimaging data. In *Proceedings of the 8th Python in Science Conference* (pp. 68-75).

Rosen, B. Q., & Halgren, E. (2021). A whole-cortex probabilistic diffusion tractography connectome. *Eneuro*, *8*(1). doi: https://doi.org/10.1523%2FENEURO.0416-20.2020

Rubinov, M., & Sporns, O. (2010). Complex network measures of brain connectivity: uses and interpretations. *Neuroimage*, *52*(3), 1059-1069. doi: https://doi.org/10.1016/j.neuroimage.2009.10.003

Saß, H., Wittchen, H. U., & Zaudig, M. (1996). *Diagnostisches und statistisches Manual psychischer Störungen-DSM-IV*. Hogrefe: Göttingen.

Supplementary Information

Setsompop, K., Gagoski, B. A., Polimeni, J. R., Witzel, T., Wedeen, V. J., & Wald, L. L. (2012). Blipped-controlled aliasing in parallel imaging for simultaneous multislice echo planar imaging with reduced g-factor penalty. *Magnetic resonance in medicine*, *67*(5), 1210-1224. doi: https://doi.org/10.1002/mrm.23097

Shen, X., Tokoglu, F., Papademetris, X., & Constable, R. T. (2013). Groupwise whole-brain parcellation from resting-state fMRI data for network node identification. *Neuroimage*, *82*, 403-415. doi: https://doi.org/10.1016/j.neuroimage.2013.05.081

Smith, S. M. (2002). Fast robust automated brain extraction. *Human brain mapping*, *17*(3), 143-155. doi: https://doi.org/10.1002/hbm.10062

Smith, S. M., Nichols, T. E., Vidaurre, D., Winkler, A. M., Behrens, T. E., Glasser, M. F., ... & Miller, K. L. (2015). A positive-negative mode of population covariation links brain connectivity, demographics and behavior. *Nature neuroscience*, *18*(11), 1565-1567. doi: https://doi.org/10.1038/nn.4125

Smith, R. E., Tournier, J. D., Calamante, F., & Connelly, A. (2012). Anatomically-constrained tractography: improved diffusion MRI streamlines tractography through effective use of anatomical information. Neuroimage, 62(3), 1924-1938. doi: https://doi.org/10.1016/j.neuroimage.2012.06.005

Tabachnick, B. G., & Fidell, L. S. (2001). Using Multivariate Statistics. *Allyn & Bacon*.

Taylor, P. A., & Saad, Z. S. (2013). FATCAT:(an efficient) functional and tractographic connectivity analysis toolbox. *Brain connectivity*, *3*(5), 523-535. doi: https://doi.org/10.1089/brain.2013.0154

Tournier, J. D., Calamante, F., & Connelly, A. (2010, May). Improved probabilistic streamlines tractography by 2nd order integration over fibre orientation distributions. In Proceedings of the international society for magnetic resonance in medicine (Vol. 1670). John Wiley & Sons, Inc, New Jersey.

Tournier, J. D., Smith, R., Raffelt, D., Tabbara, R., Dhollander, T., Pietsch, M., ... & Connelly, A. (2019). MRtrix3: A fast, flexible and open software framework for medical image processing and visualisation. *Neuroimage*, *202*, 116137. doi: https://doi.org/10.1016/j.neuroimage.2019.116137

Supplementary Information

Tustison, N. J., Avants, B. B., Cook, P. A., Zheng, Y., Egan, A., Yushkevich, P. A., & Gee, J. C. (2010). N4ITK: improved N3 bias correction. IEEE transactions on medical imaging, 29(6), 1310-1320. doi: https://doi.org/10.1109/TMI.2010.2046908

Wang, H. T., Smallwood, J., Mourao-Miranda, J., Xia, C. H., Satterthwaite, T. D., Bassett, D. S., & Bzdok, D. (2020). Finding the needle in a high-dimensional haystack: Canonical correlation analysis for neuroscientists. *NeuroImage*, *216*, 116745. doi: https://doi.org/10.1016/j.neuroimage.2020.116745

Wittchen, H. U., Wunderlich, U., Gruschwitz, S., & Zaudig, M. (1997). *SKID I. Strukturiertes Klinisches Interview für DSM-IV. Achse I: Psychische Störungen. Interviewheft und Beurteilungsheft*. Hogrefe.

Xia, C. H., Ma, Z., Ciric, R., Gu, S., Betzel, R. F., Kaczkurkin, A. N., ... & Satterthwaite, T. D. (2018). Linked dimensions of psychopathology and connectivity in functional brain networks. *Nature communications*, *9*(1), 3003. doi: https://doi.org/10.1038/s41467-018-05317-y

Xu, J., Moeller, S., Auerbach, E. J., Strupp, J., Smith, S. M., Feinberg, D. A., ... & Uğurbil, K. (2013). Evaluation of slice accelerations using multiband echo planar imaging at 3 T. *Neuroimage*, *83*, 991-1001. doi: https://doi.org/10.1016/j.neuroimage.2013.07.055

Zheng, H., Bergamino, M., Ford, B. N., Kuplicki, R., Yeh, F. C., Bodurka, J., ... & Savitz, J. (2021). Replicable association between human cytomegalovirus infection and reduced white matter fractional anisotropy in major depressive disorder. *Neuropsychopharmacology*, *46*(5), 928-938. doi: https://doi.org/10.1038/s41386-021-00971-1